IEICE TRANS. INF. & SYST., VOL.E85–D, NO.10 OCTOBER 2002

PAPER

Neural Filter with Selection of Input Features and Its Application to Image Quality Improvement of Medical Image Sequences*

Kenji SUZUKI†, **Isao HORIBA**†, **Noboru SUGIE**††, ***Regular Members***, ***and*** **Michio NANKI**†††, ***Nonmember***

SUMMARY In this paper, we propose a new neural filter to which the features related to a given task are input, called a neural filter with features (NFF), to improve further the performance of the conventional neural filter. In order to handle the issue concerning the optimal selection of input features, we propose a framework composed of 1) manual selection of candidates for input features related to a given task and 2) training with automatically selection of the optimal input features required for achieving the given task. Experiments on the proposed framework with an application to improving the image quality of medical X-ray image sequences were performed. The experimental results demonstrated that the performance on edge-preserving smoothing of the NFF, obtained by the proposed framework, is superior to that of the conventional neural and dynamic filters.

key words: *input feature, automatically selection, edge preserving, optimal input, dynamic filter*

1. Introduction

Recently, applications utilizing digital video technologies have increased dramatically in various fields such as medicine, industry, robotics, transportation systems, and so on. Accordingly, demands for noise reduction algorithms for dynamic image sequences are increasing. Especially in the medical field, noise reduction algorithms are indispensable for digital X-ray imaging systems because of the reason below. High-dose X-ray has to be used to reduce quantum noise in X-ray images. Consequently, not only patients but also medical doctors are heavily exposed to radiation. Therefore, noise reduction of the X-ray image sequences obtained at low exposure levels has been desired fervently by medical doctors. In order to improve the quality of image sequences, various dynamic filters have been proposed so far [1]–[6]. However, how to determine the optimal filter coefficients suitable for a given task has remained a serious issue in these conventional filters.

Recently, nonlinear filters based on multilayer neural networks (here referred to as NNs), called neural filters (here referred to as NFs), have been proposed. In these filters, the filtering characteristics can be determined by training with a set of input and desired teaching images [7]–[19]. Since it has been proved that any continuous mapping can be approximately realized by multilayer NNs [20], [21], we trust the NFs to have a high performance; we have continued researches on image processing using the NFs [13]–[19]. In applications of the NFs to improving the image quality of medical image sequences, the performance on preserving the edges of moving objects is not sufficient, although that on noise reduction is very high [13]–[16], [19]. Therefore, how to improve the performance on preserving edges has remained a serious issue.

In this paper, we propose a new NF to which the features related to a given task are input, called a NF with features (here referred to as NFF), to improve the performance of the conventional NF. In general, we cannot clearly know the optimal input features required for achieving the given task. In order to handle the issue concerning the optimal selection, we propose a framework composed of 1) manual selection of candidates for input features related to the given task and 2) training with automatically selection of the optimal input features required for achieving the given task.

Experiments on the proposed framework with application to improving the image quality of medical X-ray image sequences are performed. The goals of improving the image quality of medical X-ray image sequences are: (1) to remove quantum noise from low-dose X-ray images in order to reduce X-ray exposure to patients and (2) to enhance rapidly moving diagnostic objects in order to discern them clearly. To achieve these goals are exceedingly difficult for conventional dynamic filters: the quantum noise in medical X-ray images is not mare Gaussian noise but a specific type of noise called quantum mottle. The quantum mottle is caused from the effects of the compound characteristics of a measurement system. The conventional dynamic

Manuscript received October 13, 2000.
Manuscript revised March 12, 2002.

†The authors are with the Faculty of Information Science and Technology, Aichi Prefectural University, Aichi-ken, 480–1198 Japan.
††The author is with the Faculty of Science and Technology, Meijo University, Nagoya-shi, 468–8502 Japan.
†††The author is with Chubu Rosai Hospital, Nagoya-shi, 455–8530 Japan.

*This work was supported in part by the Ministry of Education, Science, Sports and Culture of Japan under grant-in-aid for quantum information theoretical approach to life science and grant-in-aid for encouragement of young scientists.

filters are developed on the assumption that noise is Gaussian. Furthermore, the objects in medical images move so rapidly in comparison with general image sequences, while the conventional dynamic filters are developed for general image sequences. Thus, the conventional dynamic filters would not be necessarily suitable for reducing noise from medical X-ray image sequences.

Below, through comparative evaluation with the conventional NF and the conventional dynamic filters, the effectiveness of the proposed framework and the NFF are shown.

2. Proposed Framework

2.1 Architecture of the NFF [22]

The architecture of the NFF is shown in Fig. 1. t_0 and T in the figure denote the time of the current frame and the time interval between frames, respectively. The NFF consists of a modified multilayer NN, in which the activation functions of the units in input, hidden and output layers are an identity function, a sigmoid function and an identity function, respectively. The inputs to the conventional NF are only pixel values in the input window. In addition to them, the features related to a given task are input to the NFF in order to improve further the performance of the conventional NF: the inputs to the NFF are an object pixel value $g(x, y, t)$,

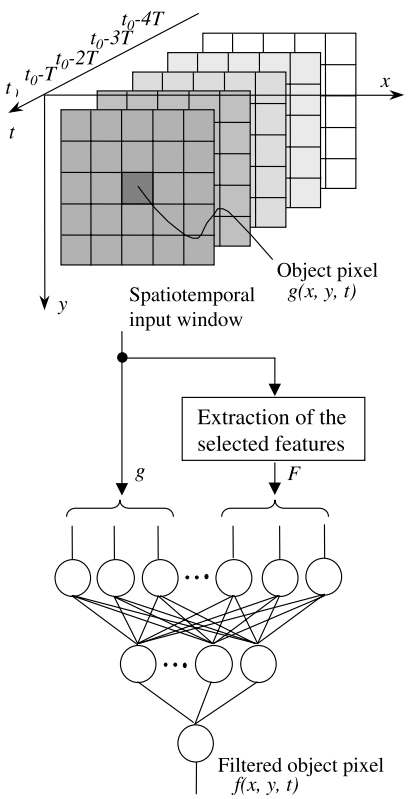

Fig. 1 Architecture of the NFF.

spatiotemporally adjacent pixel values and the features calculated from the pixel values in the input window. The output of the NFF is represented by

$$f(x, y, t) = G_M \cdot NN(\boldsymbol{I}_{x,y,t}), \tag{1}$$

$$\boldsymbol{I}_{x,y,t} = \{g(x-i, y-j, t-k), F_m(x, y, t) \mid i, j, k \in R_{ST}, 1 \le m \le M\}, \tag{2}$$

$$F_m(x, y, t) = \vartheta_m[\{g(x-i, y-j, t-k) \mid i, j, k \in R_{ST}\}] \tag{3}$$

where x and y denote the indices of spatial coordinates, t the index of temporal coordinate, $\boldsymbol{I}$ the input vector to the NFF, $NN(\boldsymbol{I})$ the output of the multilayer NN, G_M a normalization factor, R_{ST} the region of the input window, M the number of input features, F_m the mth input feature, and $\vartheta_m(\cdot)$ the operator calculating the mth input feature.

The error to be minimized by training is defined as

$$E = \frac{1}{P} \sum_p (T_C^p / G_M - O^p / G_M)^2 \tag{4}$$

where p denotes a pattern number, T_C^p the pth training data in the teaching images, O^p the pth training data in the output images, and P the number of training patterns. The NFF is trained by the modified back-propagation (BP) algorithm [23], which was derived for the above structure in the same way as the standard back-propagation algorithm [24], [25], until the following condition for stopping training is fulfilled: the error E gets smaller than or equal to the predetermined error E_P, or the number of training epochs exceeds the predetermined number T_P.

2.2 Method for Selecting Input Features

The method for designing the structure of the NF [26]–[28] is adopted as that for selecting the input features of the NFF. The input features are selected automatically under the mean square error criterion during training. An explanatory figure for the training with automatically selection of input features is shown in Fig. 2. First, we select candidates for the input features related to a given task. Next, the NFF to which the candidates are input is trained. The input features are selected on the basis of the influence of intercepting each candidate on the error. The candidate with the smallest influence is excluded first. The damage of excluding it is recovered by retraining. Excluding and retraining are performed alternately, and then the optimal input features are selected rationally.

Let m and $E^{(m)}$ define the input feature number and the error after intercepting the mth candidate for input features. The training with automatically selection of input features is composed of the following steps:

[Step 1] NFF to which the candidates for input features are input is trained.

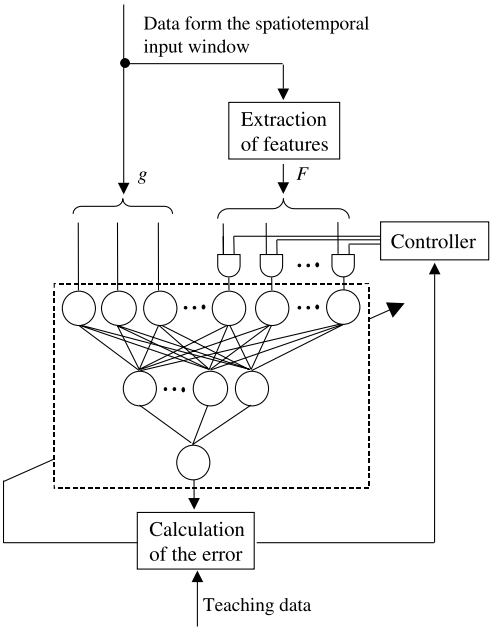

Fig. 2 Training with automatically selection of input features for the NFF.

[Step 2] Intercept the mth candidate experimentally and calculate $E^{(m)}$.

[Step 3] If every candidate is examined by intercepting it experimentally and calculating $E^{(m)}$, then go to Step 4, else go back to Step 2.

[Step 4] Exclude the ath candidate where $E^{(a)}$ is the minimum among $E^{(m)}$'s.

[Step 5] Retrain the NFF, which has been excluded the ath candidate, by the modified BP algorithm until the condition for stopping training is fulfilled.

[Step 6] If $E \leq E_P$ before the number of training epochs exceeds T_P; then memorize the weights and the structure, and go back to Step 2; else finish the steps.

The training, calculating $E^{(m)}$ and retraining in the Steps 1, 2 and 5 are performed by using the same training data set.

3. Experiments to Construct NFF for Medical Image Sequences

3.1 Method for Synthesizing Input and Teaching Images [14]

3.1.1 Synthesizing Low-dose X-ray Image Sequence

Since the X-ray quantum noise is signal-dependent Poisson-distributed noise [29], a low-dose X-ray image $g_L(x, y, t)$, an input image to the NFF, can be synthesized from a high-dose X-ray image with negligible quantum noise $g_H(x, y, t)$ as the following equations:

$$g_L(x, y, t) = g_H(x, y, t) + X_N(\sigma), \tag{5}$$

$$\sigma = k_N \sqrt{g_H(x, y, t)} \tag{6}$$

where $X_N(\sigma)$ denotes white Gaussian noise when its standard deviation is σ, and k_N a parameter determining the amount of radiation dosage.

3.1.2 Synthesizing Teaching Image Sequence

In order to restore the spatial blur caused by a measurement system, a teaching image $T_C(x, y, t)$ is synthesized from the high-dose X-ray image by performing the inverse filtering of the spatial blur $MTF^{-1}(\cdot)$ as follows:

$$T_C(x, y, t) = MTF^{-1}\{g_H(x, y, t)\}. \tag{7}$$

The parameter k_N was set to 0.24% of the maximum level of the gray scale on the basis of the actual measurement of the noise in low-dose X-ray images; $MTF^{-1}(\cdot)$ was realized on the basis of the actual measurement of a real system [30].

3.2 Construction of the NFF

3.2.1 Candidates for Input Features

Since the given task is the edge-preserving smoothing of image sequences, we selected candidates for input features correlated with spatiotemporal/spatial/temporal edges, noise reduction and the motion of objects as follows:

1) Variance of the pixel values in R_{ST},
2) Variance of the pixel values in R_S,
3) Variance of the pixel values in R_T,
4) Variance of the values projected along the time axis in R_{ST},
5) Gradient of gray levels at the object pixel [31],
6) Laplacian of gray levels at the object pixel [31],
7) Mean for the pixel values in R_{ST},
8) Mean for the pixel values in R_S,
9) Mean for the pixel values in R_T,
10) Difference between the pixel value at the object pixel in the current frame and that in the previous one

where R_{ST}, R_S and R_T denote a spatiotemporal input window, a spatial region in the current frame in R_{ST} and a temporal sequence at the same spatial coordinates of the object pixel in R_{ST}, respectively.

3.2.2 Training the NFF

The spatiotemporal input window of the NFF consisted of five pixels in each of five consecutive frames, as Fig. 1 shows. The number of units in the input, hidden and output layers were 135, 20 and 1, respectively. This structure was determined experimentally. Samples of the images used for training are shown in Fig. 3. Figures 3 (a) and (b) show the input images to the NFF.

In the figures, the current and the last frame in the input window of the NFF are shown. Figure 3 (c) shows the teaching image. These are angiograms of left coronary arteries of the heart (size: 512×480 pixels, maximum level of the gray scale: 1,024, and frame rate: 30 frames/sec.), acquired with a digital angiography system. In the figures, the edges of the images are trimmed to display the regions of interest large. In angiograms, arteries which is diagnostic objects move most rapidly of all medical image sequences. Therefore, to improve the image quality of this kind of image sequences is difficult.

The training set was made by sampling 12,000 points at random from the consecutive six frames. The predetermined number of training epochs T_P was set to 150,000 epochs. The training with automatically selection of input features was applied to the NFF. The training in the Step 1 was performed for 150,000 epochs where each epoch consists of training run of 12,000 points. The training in the Step 1 converged with the error E of 1.7%. We set the predetermined error E_P to this error, 1.7%. The redundant input features were excluded during the Steps from 2 to 6. Each retraining in the Step 5 was finished on zero to six epochs.

3.2.3 Results of Feature Selection and Discussions

The following input features were selected after applying the training with automatically selection of input features:

1) Variance of the pixel values in R_{ST}, i.e., the edge information related to motion;
6) Laplacian of gray levels at the object pixel;
8) Mean for the pixel values in R_S, i.e., a mean value robust against motion; and
10) Difference between the pixel value at the object pixel in the current frame and that in the previous one, i.e., the information related to motion.

The input features 1), 8) and 10) are the features related to motion. We considered that these features were selected because the objects in the images used for training move dynamically. The spatial characteristic of the input feature 6) is about equal to that of $MTF^{-1}(\cdot)$. We considered that this would be the reason for remaining this feature. Since the selected features 6), 8) and 10) can be calculated from the pixel values in the input window by multiplication and addition, these features seem to be redundant inputs from the theoretical point of view. However, it is not guaranteed that the NF acquires the calculation of these features through training. Indeed, the NFF from which these features had been excluded was inferior to the original NFF even if retraining was performed. This result demonstrated that the NFF is more effective than the NF from the practical point of view.

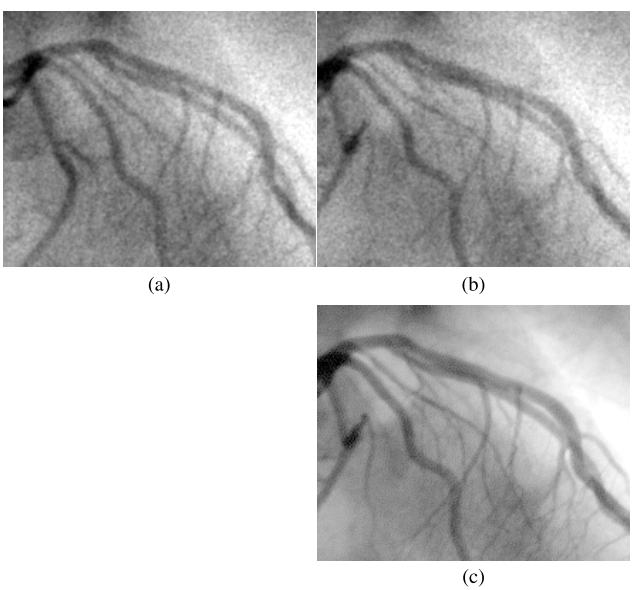

Fig. 3 Exsamples of the images used for training (Angiograms of left coronary arteries of the heart). (a) Simulated low-dose X-ray image, the last frame in the input window of the NFF $g(x, y, t_0 - 4T)$. (b) Simulated low-dose X-ray image, the current frame in the input window of the NFF $g(x, y, t_0)$. (c) Teaching image $T_C(x, y, t_0)$.

4. Comparative Evaluation

4.1 Comparison with the Conventional NF

4.1.1 Image Quality of Output Images

The performance of the NFF is compared with that of the conventional NF. To compare the performances of these filters under the same conditions, all parameters of the conventional NF were set to the same ones as the NFF except for the input features, i.e., the NF was trained using the same training set; the number of input units of the conventional NF was 125 (135 – ten input features). The output images of the conventional NF and the NFF are shown in Figs. 4 (a) and (b), respectively. In the output image of the conventional NF, the edges of the arteries, which are a diagnostic region, are

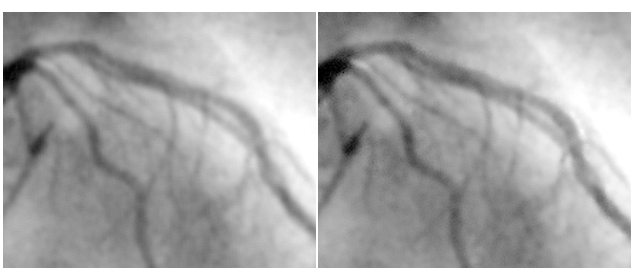

Fig. 4 Comparison of the output image of the NFF with that of the conventional NF. (a) Output image of the conventional NF. (b) Output image of the NFF.

blurred spatially. In contrast, the edges in the output image of the NFF are sharper.

4.1.2 Filter Characteristic

In order to clarify the filter characteristic of edge-preserving smoothing, the DQE (Detective Quantum Efficiency) [32], [33] was adopted as a metric. The DQE is defined as

$$DQE(h) = \frac{MTF^2(h)}{WS(h)} = \frac{|S(h)|^2}{|N(h)|^2} \quad (8)$$

where h denotes the spatial frequency, $WS(h)$ the Winner spectrum, $MTF(h)$ the modulation transfer function of a system, $S(h)$ that of the system to which only signals (but noise) are input, and $N(h)$ that of the system to which only noise is input [34]. The DQE expresses the filter's transfer function of the squired signal-to-noise ratio. The results of measurement of the DQE are shown in Fig. 5. In contrast to the conventional NF, the DQEs from middle to high frequency of the NFF are higher. This result indicates that the performance on edge-preserving smoothing of the NFF is higher than that of the conventional NF. The DQE around 0.25 of frequencies are lower than the others are. This is due to the convolution with a small local window.

4.2 Comparative Evaluation with the Conventional Dynamic Filters

4.2.1 Image Quality of Output Images

We compare the NFF with the motion-adaptive recursive filter (MARF) [3] and the adaptive weighted averaging filter (AWAF) [2]. The MARF is a kind of recursive filters. In the MARF, a parameter determining the quantity of noise reduction is adaptive to the estimated motion. The MARF is utilized for a video processing system for medical X-ray image sequences, which is widely used in hospitals. The AWAF is developed for noise suppression in image sequences without spatial blur. This is a well-known representative as a filter with good performance.

To compare the performance of the NFF with those of the conventional filters fairly, the parameters of the conventional filters were determined carefully. The parameters of the MARF were set to those used in real systems. These had been determined by a large number of tests in clinical evaluations. According to the method for determining the parameters of the AWAF in [2], the parameters were determined by using amount of noise in the input image sequence used in this experiment.

Output images of the NFF and the conventional dynamic filters in filtering the non-training images are shown in Fig. 6. Figure 6 (a) shows the current frame in the input image sequence. Figure 6 (b) indicates the motion of arteries, which is the image subtracted between consecutive two frames of the high-dose X-ray image sequence. In the output image of the MARF, the contrast of moving arteries is low. We cannot discern the moving arteries well due to blurring. In this kind of images, the contrast of the moving arteries is

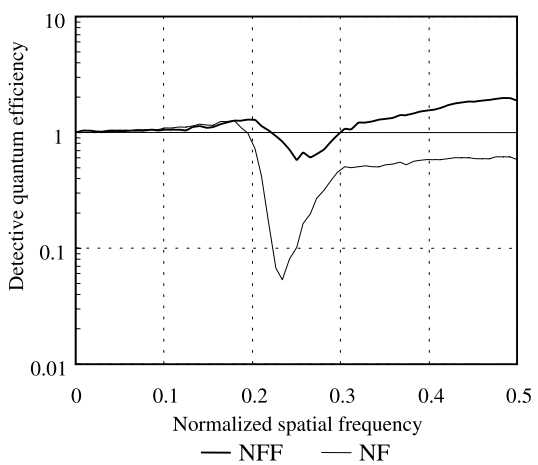

Fig. 5 Comparison of the performance on edge-preserving smoothing of the NFF with that of the conventional NF.

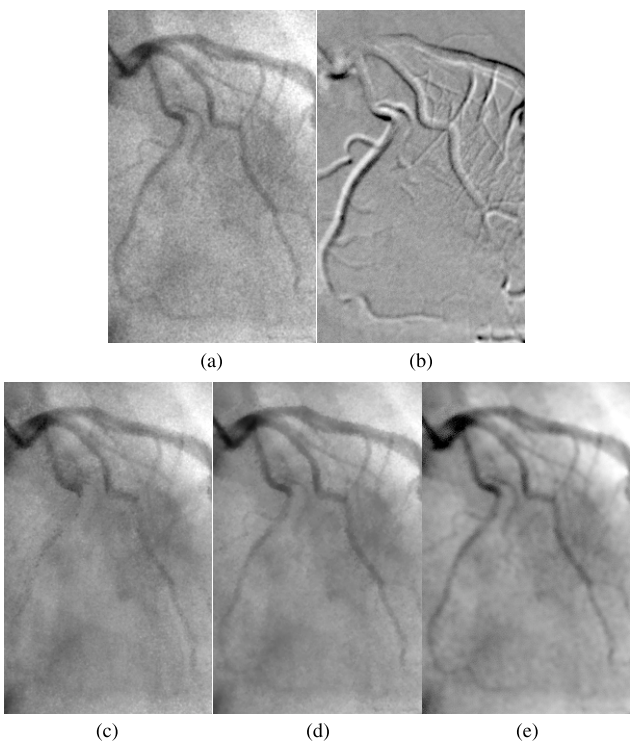

Fig. 6 Comparison of the output image of the NFF with those of the conventional dynamic filters in filtering non-training image. (a) Current frame in the input image sequence. (b) Motion of arteries. (c) Output image of the MARF. (d) Output image of the AWAF. (e) Output image of the NFF.

extremely important, because medical doctors diagnose some diseases on the basis of the state of the motion of moving arteries. In the output image of the AWAF, the contrast of the moving arteries is also low. Although the edges of arteries seem to be sharper, they are slightly over-correction and unnatural. This result is not desirable: the shape of artery is extremely important, because medical doctors diagnose stenosis, a kind of heart disease, on the basis of them. In contrast, the quality of the output image of the NFF is better in terms of the contrast of the moving arteries, the shape of arteries and noise reduction.

4.2.2 Quantitative Comparisons

To compare more precisely, the image quality is evaluated quantitatively using the blurred signal-to-noise ratio (BSNR) and the improvement in signal-to-noise ratio (ISNR) [35], [36]. These metrics are widely used in evaluation of the performances of image restoration techniques and dynamic filters. The BSNR expresses the signal-to-noise ratio of input images, and the ISNR expresses the improvement in signal-to-noise ratio from the signal-to-noise ratio of input images. The BSNR and the ISNR are defined as

$$BSNR(t) = 10\log_{10}\frac{\sum_{x,y\in R_E}\{T_C(x,y,t)-\overline{T_C(x,y,t)}\}^2}{\sum_{x,y\in R_E}\{Ns(x,y,t)-\overline{Ns(x,y,t)}\}^2} \quad (9)$$

where

$$Ns(x,y,t) = g(x,y,t) - f(x,y,t), \quad (10)$$

R_E denotes a region for evaluation, $Ns(x,y,t)$ noise in the input image, $\overline{T_C(x,y,t)}$ and $\overline{Ns(x,y,t)}$ means for $T_C(x,y,t)$ and $Ns(x,y,t)$, respectively;

$$ISNR(t) = 10\log_{10}\frac{\sum_{x,y\in R_E}\{T_C(x,y,t)-g(x,y,t)\}^2}{\sum_{x,y\in R_E}\{T_C(x,y,t)-f(x,y,t)\}^2}. \quad (11)$$

Furthermore, to evaluate the performance on the motion of objects, the MEF (Motion in Each Frame) was adopted. The MEF is defined as a mean for differences of pixel values between consecutive two frames in the high-dose X-ray images $g_H(x,y,t)$:

$$MEF(t) = \frac{\sum_{x,y\in R_E}\left\{S(x,y,t)-\overline{S(x,y,t)}\right\}^2}{N_E\cdot G_M} \quad (12)$$

$$S(x,y,t) = g_H(x,y,t) - g_H(x,y,t-T) \quad (13)$$

where N_E denotes the number of pixels in the region for evaluation R_E, and $\overline{S(x,y,t)}$ a mean for $S(x,y,t)$.

R_E was set to the region including the whole arteries. The average BSNR, i.e., the signal-to-noise ratio of the input images, was 14.4 dB. The results of calculation of the ISNRs and the MEF are shown in Fig. 7. The images of the frame numbers from 38 through 43 were used in the training. The ISNRs of the NFF are the highest in not only training frames but also non-training ones. The average ISNRs of the NFF, NF, AWAF and MARF are 6.5, 5.4, 2.9 and 0.6 dBs, respectively. By comparing the ISNR with the MEF, it is indicated that the image quality of the output images of the AWAF depends on the motion of objects, whereas the NFF is, relatively, robuster against motion.

4.3 Evaluation with Real Low-Dose X-ray Images

4.3.1 Low-Dose X-ray Image Sequences

Since the NFF was trained using the simulated low-dose X-ray images, the evaluation with real low-dose X-ray images is important. The NFF and the conventional dynamic filters were applied to real low-dose X-ray images. The input image sequence and the output image sequences of the filters are shown in Fig. 8. These images are angiograms of left coronary arteries of the heart (size: 512×480 pixels; maximum level of the gray scale: 1,024; and frame rate: 30 frames/sec.), acquired at a low X-ray exposure level (tube voltage: 58 kV; tube current: 1.6 mA) on a digital angiography system. In the figures, the edges of images are trimmed to display the regions of interest large.

4.3.2 Image Quality of Output Images

In the output image of the MARF, the contrast of moving arteries is too low to discern them. In the output image of the AWAF, we cannot discern not only the edges of the moving arteries but also the arteries themselves due to burring. It may be difficult for medical doctors to diagnose heart disease from these images. In contrast, the quality of the output image of the NFF is better: the contrast of the moving arteries is higher, the edges and the shapes of them can be discernible, and the performance of noise reduction is better.

4.3.3 Subjective Evaluation

In order to evaluate the image quality more practically, the output images of the NFF and the conventional dynamic filters were loaded into a real digital angiography system in a hospital, and were evaluated by medical doctors (cardiologists). The processed image sequences were displayed under the same condition as a common clinical use. By the evaluation, it was confirmed that there was no artifact disturbing diagnosis in the output images of the NF and NFF. As a result, the medical doctors judged that the image quality of output image

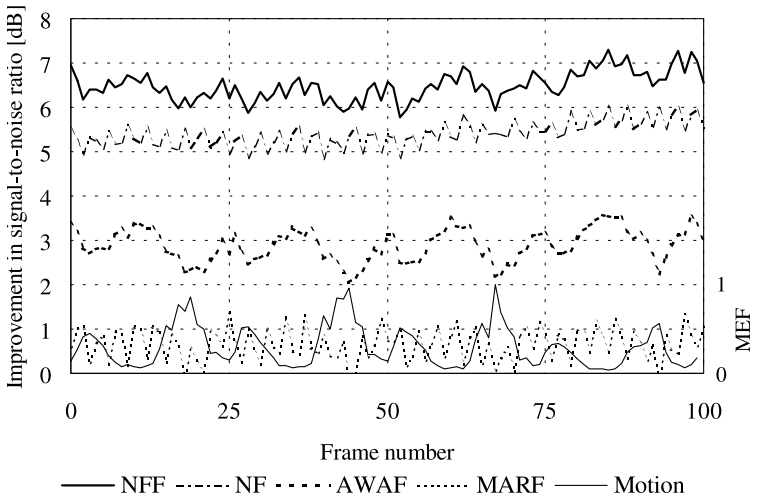

Fig. 7 Quantitative evaluation of the image quality among the output images of the filters.

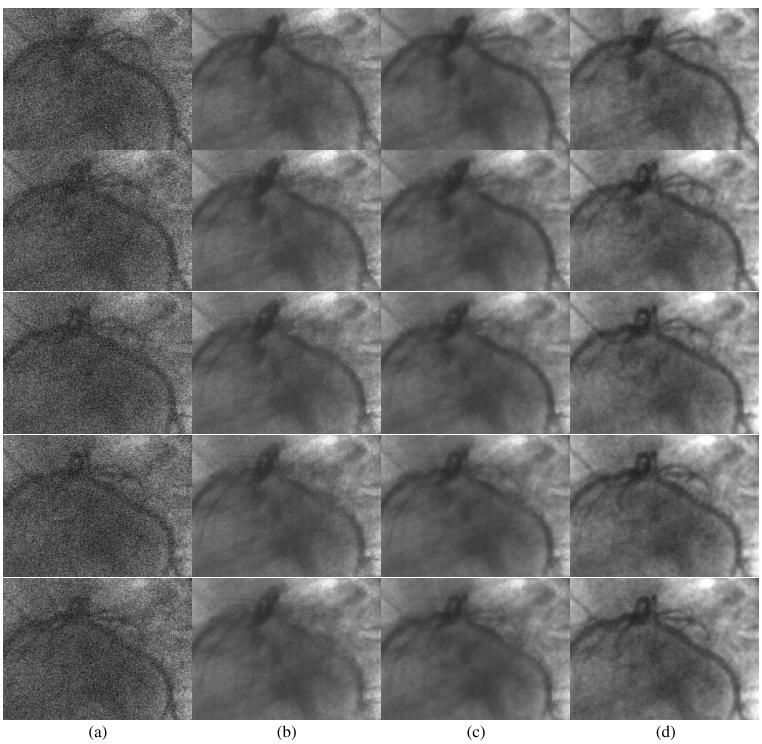

Fig. 8 Comparison of the output image sequence of the NFF with those of the conventional dynamic filters in filtering real low-dose image sequence (from top row to bottom row: $t = 38T \sim 42T$). (a) Original image sequence. (b) Output image sequence of the MARF. (c) Output image sequence of the AWAF. (d) Output image sequence of the NFF.

sequences of the NFF was superior to those of other filters: they could watch arteries much easier in the output image sequences of the NFF even in the case where these arteries moved rapidly.

5. Conclusions

In this paper, we have proposed a new NF, called the NF with features, to improve the performance of the NF and a framework for designing the NFF, which can select the optimal input features under the mean square error criterion. Experiments on the proposed framework with application to improving the image quality of medical X-ray image sequences were performed. The experimental results demonstrated that the performance on edge-preserving smoothing of the NFF is

superior to that of the conventional NF. By the quantitative evaluation, it was shown that the performance of the NFF is superior to those of the conventional dynamic filters. Through the experiments, the proposed framework has proved to be useful to design the desired NFFs.

We plan in the near future to apply the proposed framework and the NFF to various kinds of images such as natural images, traffic images, sonar images, radar images, and so on, and evaluate the performance and the versatility.

Acknowledgment

The authors wish to thank Shigenobu Yanaka, Kouichi Koike, Ken Ishikawa and Shigeyuki Ikeda of Hitachi Medical Corporation for their valuable suggestions.

References

[1] M.K. Ozkan, A.T. Erdem, M.I. Sezan, and A.M. Tekalp, "Efficient multiframe Wiener restoration of blurred and noisy image sequences," IEEE Trans. Image Processing, vol.1, no.4, pp.453–476, Oct. 1992.

[2] M.K. Ozkan, M.I. Sezan, and A.M. Tekalp, "Adaptive motion-compensated filtering of noisy image sequences," IEEE Trans. Circuits & Syst. for Video Tech., vol.3, no.4, pp.277–290, Aug. 1993.

[3] K. Enomoto, T. Hayashi, I. Horiba, K. Ikegaya, and M. Nanki, "Improving image quality of X-ray fluoroscopy," Proc. 1993 Tokai-Sec. Joint Conf. Seven Inst. Elec. Relat. Eng., p.731, 1993.

[4] C.L. Chan, A.K. Katsaggelos, and A.V. Sahakian, "Image sequence filtering in quantum-limited noise with applications to low-dose fluoroscopy," IEEE Trans. Med. Imaging, vol.12, no.3, pp.610–621, March 1993.

[5] R. Aufrichtig and D.L. Wilson, "X-ray fluoroscopy spatiotemporal filtering with object detection," IEEE Trans. Med. Imaging, vol.14, no.4, pp.733–746, April 1995.

[6] J.C. Brailean, R.P. Kleihorst, S. Efstratiadis, A.K. Katsaggelos, and R.L. Lagendijk, "Noise reduction filters for dynamic image sequences: A review," Proc. IEEE, vol.83, no.9, pp.1270–1292, Sept. 1995.

[7] K. Arakawa and H. Harashima, "A nonlinear digital filter using multi-layered neural networks," Proc. IEEE Int. Conf. Commun., vol.2, pp.424–428, 1990.

[8] K. Arakawa and H. Harashima, "Design of layered-neural nonlinear filters using back-propagation algorithm," IEICE Trans. Fundamentals (Japanese Edition), vol.J74-A, no.3, pp.421–429, March 1991.

[9] L. Yin, J. Astola, and Y. Neuvo, "A new class of nonlinear filters - neural filters," IEEE Trans. Signal Processing, vol.41, no.3, pp.1201–1222, March 1993.

[10] L. Yin, J. Astola, and Y. Neuvo, "Adaptive multistage weighted order statistic filters based on the back propagation algorithm," IEEE Trans. Signal Processing, vol.42, no.2, pp.419–422, Feb. 1994.

[11] Z.Z. Zhang and N. Ansari, "Structure and properties of generalized adaptive neural filters for signal enhancement," IEEE Trans. Neural Networks, vol.7, no.4, pp.857–868, July 1996.

[12] H. Hanek and N. Ansari, "Speeding up the generalized adaptive neural filters," IEEE Trans. Image Processing, vol.5, no.4, pp.705–712, May 1996.

[13] K. Suzuki, I. Horiba, N. Sugie, and S. Ikeda, "Improvement of image quality of X-ray fluoroscopy using spatiotemporal neural filter which learns noise reduction and edge enhancement," Proc. Int. Conf. Signal Proc. Appli. and Tech., vol.2, pp.1382–1386, Oct. 1996.

[14] K. Suzuki, I. Horiba, N. Sugie, and M. Nanki, "Noise reduction of medical X-ray image sequences using a neural filter with spatiotemporal inputs," Proc. Int. Symp. Noise Reduction for Imaging & Commun. Syst., pp.85–90, Nov. 1998.

[15] K. Suzuki, I. Horiba, and N. Sugie, "Efficient approximation of a neural filter for quantum noise removal in X-ray images," Neural Networks for Signal Processing IX, pp.370–379, IEEE Press, Piscataway, NJ, 1999.

[16] K. Suzuki, I. Horiba, and N. Sugie, "An analysis of the neural filter trained to improve quality of images with quantum noise and realization of approximate filter," Trans. IPSJ, vol.41, no.3, pp.711–721, March 2000.

[17] K. Suzuki, I. Horiba, and N. Sugie, "Signal-preserving training for neural networks for signal processing," Proc. IEEE Int. Symp. Intelligent Signal Proc. and Commun. Syst., vol.1, pp.292–297, Nov. 2000.

[18] K. Suzuki, I. Horiba, and N. Sugie, "Training under achievement quotient criterion," Neural Networks for Signal Processing X, pp.537–546, IEEE Press, Piscataway, NJ, 2000.

[19] K. Suzuki, I. Horiba, and N. Sugie, "Efficient approximation of neural filters for removing quantum noise from images," IEEE Trans. Signal Processing, vol.50, no.7, pp.1787–1799, July 2002.

[20] K. Funahashi, "On the approximate realization of continuous mappings by neural networks," Neural Networks, vol.2, pp.183–192, 1989.

[21] A.R. Barron, "Universal approximation bounds for superpositions of a sigmoidal function," IEEE Trans. Inf. Theory, vol.39, no.3, pp.930–945, March 1993.

[22] K. Suzuki, I. Horiba, N. Sugie, and M. Nanki, "Improving image quality of medical image sequences using a neural filter with selection of input features," Trans. IPSJ, vol.42, no.8, pp.2176–2188, 2001.

[23] K. Suzuki, I. Horiba, K. Ikegaya, and M. Nanki, "Recognition of coronary arterial stenosis using neural network on DSA system," Systems and Computers in Japan, vol.26, no.8, pp.66–74, Aug. 1995.

[24] D.E. Rumelhart, G.E. Hinton, and R.J. Williams, "Learning representations of back-propagation errors," Nature, vol.323, pp.533–536, 1986.

[25] D.E. Rumelhart, G.E. Hinton, and R.J. Williams, "Learning internal representations by error propagation," vol.1 of Parallel Distributed Processing, chapter 8, pp.318–362, MIT Press, MA, 1986.

[26] K. Suzuki, I. Horiba, and N. Sugie, "Designing the optimal structure of a neural filter," Neural Networks for Signal Processing VIII, pp.323–332, IEEE Press, Piscataway, NJ, 1998.

[27] K. Suzuki, I. Horiba, and N. Sugie, "A method for determining reduced structure of a neural filter," Trans. IPSJ, vol.40, no.12, pp.4226–4238, Dec. 1999.

[28] K. Suzuki, I. Horiba, and N. Sugie, "A simple neural network pruning algorithm with application to filter synthesis," Neural Processing Letters, vol.13, no.1, pp.43–53, Feb. 2001.

[29] A. Macovski, Medical Imaging Systems, PrenticeHall, Englewood Cliffs, NJ, 1983.

[30] F. Takahashi, K. Ishikawa, and T. Taniguchi, et al., "Development of a high definition real-time digital radiography system using a 4 million pixels CCD camera," Proc. SPIE Medical Imaging, vol.3032, pp.364–375, Feb. 1997.

[31] A. Rosenfeld and A.C. Kak, Digital Picture Processing, 2nd ed., vol.2, pp.84–96, Academic Press, 1982.
[32] R. Nishikawa and M.J. Yaffe, "Effect of various noise sources on the detective quantum efficiency of phosphor screens," Medical Physics, vol.17, no.5, pp.887–893, 1990.
[33] R. Nishikawa and M.J. Yaffe, "Model of the spatial-frequency-dependent detective quantum efficiency of phosphor screens," Medical Physics, vol.17, no.5, pp.894–904, 1990.
[34] A.V. Oppenheim and A.S. Willsky, Signal and Systems, 2nd ed., pp.226–231, Prentice-Hall, NJ, 1997.
[35] M.R. Banham and A.K. Katsaggelos, "Digital image restoration," IEEE Signal Processing Magazine, vol.14, no.2, pp.24–41, March 1997.
[36] J.C. Brailean, R.P. Kleihorst, S. Efstratiadis, A.K. Katsaggelos, and R.L. Lagendijk, "Noise reduction filters for dynamic image sequences: A review," Proc. IEEE, vol.83, no.9, pp.1270–1291, Sept. 1995.

Kenji Suzuki was born in Nagoya, Japan, in 1968. He received the B.S. and M.S. degrees, both with highest honors, in electrical and electronic engineering from Meijo University, Nagoya, Japan, in 1991 and 1993, respectively, and the Ph.D. degree in information engineering by a thesis from Nagoya University, Nagoya, Japan, in 2001. From 1993 to 1997, he was with the Research and Development Center at Hitachi Medical Corporation, Kashiwa, Japan, as a Researcher. He was engaged in research and development of intelligent medical imaging systems, including a digital subtraction angiography system and a digital radiography system. In 1997, he joined Aichi Prefectural University, Aichi, Japan, where he assisted in founding the Faculty of Information Science and Technology. From 1998 to 2002, he was with the Faculty of Information Science and Technology at Aichi Prefectural University as a Research Associate. Since 2002, he has been a Research Associate in the Kurt Rossmann Laboratories for Radiologic Image Research, the Department of Radiology, the Division of Biological Sciences, the University of Chicago, IL, USA.

Isao Horiba was born in Nagoya, Japan, in 1948. He received the B.S. and Ph.D. degrees in electrical engineering from Nagoya University, Nagoya, Japan, in 1974 and 1985, respectively. From 1974 to 1987, he was with the Research and Development Center at Hitachi Medical Corporation, Kashiwa, Japan, as a Senior Researcher. He was engaged in development of computed topography systems, magnetic resonance imaging systems, digital subtraction angiography systems, digital radiography systems, and so on. In 1987, he joined the Faculty of Science and Technology at Meijo University, Nagoya, Japan, as an Assistant Professor and then an Associate Professor. He has been a Professor in the Faculty of Information Science and Technology at Aichi Prefectural University, Aichi, Japan, since 1998.

Noboru Sugie was born in Nagoya, Japan, in 1932. He received the B.S. degree in electrical engineering from Nagoya University, Nagoya, Japan, in 1957, and the Ph.D. degree in engineering from the University of Tokyo, Tokyo, Japan, in 1970. From 1957 to 1979, he was with the Government Electrotechnical Laboratory, Tsukuba, Japan. During the period of 1962 to 1964, he was on leave with the Department of Electrical Engineering, McGill University, Montreal, Canada as an NRC Postdoctoral Fellow. He was the director of the sections of bionics and human vision at the Government Electrotechnical Laboratory, from 1970 to 1977, from 1977 to 1978, respectively. From 1979 to 1994, he was a Professor in the Department of Information Engineering and the Graduate School of Engineering at Nagoya University. From 1990 to 1994, he was the director of Nagoya University Computation Center. He was a professor emeritus of Nagoya University. From 1994 to 2000, he was a Professor in the Department of Electrical and Electronic Engineering and the Graduate School of Science and Technology at Meijo University, Nagoya, Japan. Since 2000, he has been the founding Chairman of the Department of Information Sciences and Technology.

Michio Nanki was born in Japan, in 1950. He received the M.D. degree from Nagoya University, Nagoya, Japan, in 1976. From 1976 to 1979, he was with Shizuoka Saiseikai Hospital. From 1979 to 1982, he was with the Circulatory Research Laboratory in the Third Department of Internal Medicine at Nagoya University Hospital. From 1982 to 1985, he was with the Cardiovascular Internal Medicine at the National Cardiovascular Center. From 1985 to 1999, he was a director of the Division of Internal Medicine at Chubu Rosai Hospital, Nagoya, Japan. From 1999 to 2000, he was the founding director of the Division of Cardiovascular Medicine at Chubu Rosai Hospital. Since 2000, he has been a Vice President of Chubu Rosai Hospital.